ELSEVIER

Energy and Buildings 32 (2000) 327–343

ENERGY AND BUILDINGS

www.elsevier.com/locate/enbuild

Turbulent airflow in a room with a two-jet heating-ventilation system — a numerical parametric study

J.J. Costa [a,*], L.A. Oliveira [a], D. Blay [b]

[a] *Dep. Engenharia Mecânica, Universidade de Coimbra — Polo II, 3030 Coimbra, Portugal*
[b] *Laboratoire d'Etudes Thermiques, E.N.S.M.A. — BP 109, 86960 Futuroscope Cedex, France*

Accepted 30 March 2000

Abstract

The two-dimensional turbulent airflow generated by two non-isothermal plane wall jets in a compartment is numerically investigated over a wide range of supply airflow rates. The low-Reynolds-number turbulence model of Nagano and Hishida, assembled in a finite-volume-based numerical code, is used after a previous validation study involving several other formulations of the $k-\varepsilon$ model.

The results of an extensive parametric study are reported and discussed, and conclusions are drawn about the relative influences of the room aspect ratio, the jet inlet sections, the temperature of the walls and the ratio of ventilation-to-heating airflow rates on the flow structure and the maximum velocity in the return flow. Evidence is provided that the common requirements of ventilation rate in non-industrial buildings imply airflows that lie within a mixed convection regime, where deep changes of the flow pattern can occur. Attention is given to the parametric conditions associated with flow reversal, a situation that can seriously compromise thermal comfort. In fact, the maximum velocity in the occupied zone may then double for the same ventilation rate.

Keywords: Airflow; Heating-ventilation system; Low-Reynolds-number turbulence model

1. Introduction

Turbulent recirculating airflows generated by wall jets are frequently found in the domain of room heating and ventilation, where numerical methods have become a suitable and popular basis for analysis and design. The accuracy of the numerical approach relies greatly on the ability of the associated turbulence model to reproduce the turbulent features of momentum and heat transport.

As reviewed by Chen and Jiang [1], the high-Reynolds $k-\varepsilon$ turbulence model [2] has been widely used to study the field distributions of air velocity, temperature, turbulence intensity, relative humidity, contaminant concentration and the air quality within ventilated spaces. The dissertations of Nielsen [3] and of Restivo [4] were perhaps the earliest studies of confined turbulent flows generated by wall jets, having a close relevance for ventilation problems. The physical model corresponds to a room with a mixing flow heating–ventilation system, where fresh air is supplied by either a two- or a three-dimensional horizontal, rectangular wall jet beneath the ceiling, the exhaust section is located down in the opposite wall and heat is uniformly supplied through the floor. As reported in Ref. [4], experiments were carried out in a 1/30 scale model, and included LDA measurements and flow visualisation of isothermal flows. Three different geometries of the jet inlet section were considered, producing from essentially 2-D to 3-D flows that were analysed in a regime ($Re_j = 5000$–9000) where the flow structures were practically Reynolds-independent (self-similar flows).

Restivo [4] also reported 2-D and 3-D numerical simulations, using the *standard* high-*Re* $k-\varepsilon$ turbulence model with wall-functions. A parametric study for isothermal conditions led him to conclude that (cf. also Refs. [5–7]): (i) the maximum velocity in the return flow (U_{rm}) is determined, not by the shape, but by the area of the jet inlet section (a_0), provided that its global dimensions are small; (ii) for a constant-supply air velocity, U_{rm} increases approximately with a_0 and decreases with the room length (L). (iii) Considering a fixed supply airflow rate (e.g., imposed by the ventilation requirements, in a practical situation), it was concluded that U_{rm} tends to vary in-

* Corresponding author.

0378-7788/00/$ - see front matter
PII: S0378-7788(00)00056-6

versely with the square root of a_0. For non-isothermal flows, Restivo [4] concluded that the buoyancy effects should be included both in the momentum equation and in the terms of production/destruction of turbulence energy. Results of 2-D calculations showed that U_{rm} increased with the thermal load. Beyond a certain level, the wall jet started to separate more and more prematurely from the ceiling, until it finally originated a total flow reversal. In addition, Restivo [4] concluded that the ratio of the room length-to-height (L/H) had a relatively small influence on the critical conditions that determine the flow reversal.

Whittle [8] used 2-D numerical calculations to investigate the air movement and convective heat transfer in a similar configuration with a window beneath the ventilation (horizontal) wall jet. Higher air velocities were found in the occupied zone for a summer configuration, due to the assisting buoyancy effects. On the contrary, winter conditions produced a flow pattern that was divided at approximately mid-height into two counter-rotating cells, as a result of the adverse buoyancy forces in the window vicinity. Using also the finite-volume method [9] and the *standard* k–ε turbulence model, Skovgaard and Nielsen [10] performed a 3-D numerical study of the isothermal airflow generated in a full-scale room ($4.2 \times 3.6 \times 2.4$ m^3, thus with $L/H = 1.75$) by a rectangular horizontal jet, located in the symmetry plane at an end-wall and near the ceiling. Considering two different geometries of the jet section (0.3×0.35 and 0.3×0.23 m^2), calculations covered the range of 2200–22500 of the jet Reynolds number (Re_j, based on a_0), corresponding to $N_{ac} \approx 1$–11 air changes per hour. The 3-D characteristics of the flow were evidenced by the location of U_{rm}: not in the symmetry plane, but near the side walls. Furthermore, the results verified the simplified models that are frequently used in the design of mixing flow ventilation systems:

$$U_{rm} = c_1 N_{ac} \tag{1a}$$

and

$$U_{rm} = c_2 \sqrt{M_0} \tag{1b}$$

where M_0 is the jet momentum and c_1 and c_2 are constants. These relations are valid for fully turbulent flows and limited to the same room geometry (L/H). An alternative, apparently more general expression was suggested:

$$U_{rm} = f_L U_j K_u \frac{\sqrt{a_0}}{L + x_0} \tag{1c}$$

where x_0 is the distance to the virtual origin of the jet, K_u is a constant depending on the type and geometry of the supply air terminal, and f_L is a function only of the two- or three-dimensional character of the jet flow, when it hits the opposite wall. For the two jet geometries, respectively, the values 3.9 and 4.2, for K_u, and 0.435 and 0.42 for f_L, are reported in Ref. [10] (determined with the assumption of $x_0 = 0$). For nearly 2-D flows, a value of $f_L \approx 0.7$ is referred in Ref. [11].

These simplified models lose validity for lower flow regimes. Due to the effects of low turbulence level, the airflow pattern can no more be considered self-similar, and the design parameters will be Reynolds-dependent. In fact, most situations in room heating and ventilation of non-industrial buildings involve low velocity airflows, that are neither fully turbulent and developed nor completely laminar, and may lie in a mixed-convection flow regime. Turbulence models that account for low-Reynolds-number and near-wall turbulence decay effects should therefore be used. Over the past two decades, several different versions of the so-called "low-*Re*" k–ε turbulence model have been proposed and extensively tested in a variety of isothermal boundary layer [12] and ventilation [13] problems, and in natural convection flows [14,15]. The application of such models to mixed-convection recirculating flows, like those commonly occurring in room ventilation, has however been scarcer [16–18].

In a recent work by the authors [19], the problem of the 2-D confined, mixed convection airflow generated by two non-isothermal plane wall jets was investigated numerically and experimentally. Measurements of the turbulent velocity and temperature fields in a 1×1 m^2 cross-section cavity were reported. Eight low-Reynolds-number k–ε turbulence models were comparatively tested, together with a simplified version of the two-layer wall-function model of Chieng and Launder [20]. The latter achieved a rather satisfactory performance when used with the same fine grid that placed all the wall-adjacent nodes well inside the viscous sublayer (max $x_n^+ < 0.45$). However, the best overall approach to the experimental data was achieved with the low-*Re* model of Nagano and Hishida [21]. Its results were still improved by varying the turbulent Prandtl number, Pr_t, and the "constant" $C_{\varepsilon 3}$ in the ε equation, according to appropriate functions.

This methodology was thus successfully validated and has been used with confidence in our subsequent calculations. In the present work, an extensive program of systematic 2-D calculations is reported, aiming to study the influences of the relevant geometric, dynamic and thermal parameters on the flow and heat transfer characteristics over a wide range of airflow rates. The physical model, schematically represented in Fig. 1, can be identified as a mixing flow heating–ventilation system, where fresh air is horizontally injected adjacent to the ceiling, and heat is supplied by a warm vertical wall jet at the floor level. Analysis of results is greatly based on the dimensional plots of the maximum velocity in the occupied zone, represented by U_{rm}, against the ventilation rate, N_{ac}, which allow to clearly identify the different flow regimes: natural, mixed and forced convection. The flow field details are mostly illustrated as streamline patterns, giving emphasis to the mixed convection regime and the structural

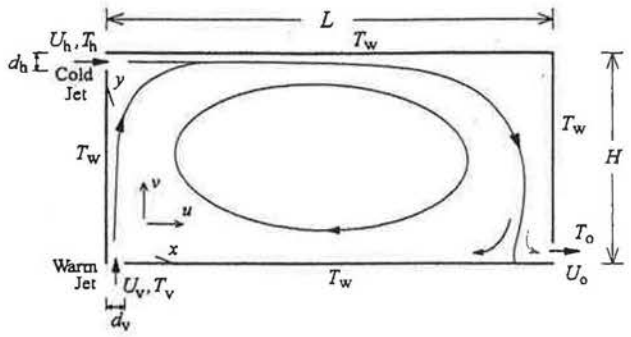

Fig. 1. Geometric configuration of the heating–ventilation system.

changes associated with the buoyancy-induced flow reversal.

2. Numerical method

In order to simplify the problem, the confined turbulent airflow was considered to be 2-D, incompressible, steady-state in average and the Boussinesq approximation [22] was assumed for the fluid physical properties.

The numerical method is based on the solution of the Reynolds-averaged equations for the conservation of mass, momentum and thermal energy. In analogy with laminar flow, the turbulent stresses and heat fluxes that arise in these equations are related to the mean velocity and temperature gradients through the Boussinesq concept of turbulent viscosity, ν_t. In the k–ε turbulence model, ν_t is obtained from the usually called Prandtl–Kolmogorov relation:

$$\nu_t = f_\mu C_\mu K^2/\tilde{\varepsilon} \tag{2}$$

thus implying the solution of two further transport equations for the turbulent kinetic energy, k, and its dissipation rate, ε (or $\tilde{\varepsilon}$, cf. Table 1). The set of equations to be solved can be cast into the generalised conservation equation (cf. Nomenclature for further symbol identification):

$$\frac{\partial}{\partial x_j}(u_j\phi) = \frac{\partial}{\partial x_j}\left(\Gamma_\phi \frac{\partial \phi}{\partial x_j}\right) + S_\phi \tag{3}$$

where the diffusibility Γ_ϕ and the source-term S_ϕ take the different meanings indicated in Table 1, according to the dependent variable represented by ϕ.

The terms P_k and G_k in the k and $\tilde{\varepsilon}$ equations represent the rates of shear production and buoyancy production/destruction of turbulence energy, respectively. As listed in Table 1, the transport equations are written in the general low-Reynolds-number form of the k–ε turbulence model. They differ from their basic version in the high-*Re* model [2] by the inclusion of (i) the viscous diffusion terms in all transport equations, (ii) the modifying functions f that make the terms containing constants C dependent upon the local level of turbulence and, in some cases, (iii) additional terms denoted by D_k and E_ε in the k and $\tilde{\varepsilon}$ equations, respectively, to better represent the near-wall behaviour of turbulence. After previous validation tests involving several other formulations [19], the low-*Re* model proposed by Nagano and Hishida (NH) [21], and specified in Table 2, was selected for the present calculations, incorporating the following expressions for the turbulent Prandtl number Pr_t and the "constant" C_{ε_3} (Refs. [23,24], respectively):

$$Pr_t = \frac{\kappa\left[1-\exp\left(-x_n^+/A^+\right)\right]}{\kappa'\left[1-\exp\left(-x_n^+/B^+\right)\right]} \tag{4}$$

$$C_{\varepsilon_3} = \tanh|\nu/u| \tag{5}$$

where $A^+ = 26$, $B^+ = 50$ and $\kappa' = \kappa/0.55$.

The partial differential equations were discretized using the finite-volume method described in Ref. [9] and the

Table 1
Values of Γ_ϕ and S_ϕ in the general transport equation (3)

Transported property	ϕ	Γ_ϕ	S_ϕ
Mass	1	0	0
Momentum in i-direction	u_i	$\nu_{ef} = \nu + \nu_t = \nu + f_\mu C_\mu \frac{k^2}{\tilde{\varepsilon}}$	$-\frac{1}{\rho}\frac{\partial p_{ef}}{\partial x_i} - g_i\beta(T - T_{ref}) + \frac{\partial}{\partial x_j}\left(\nu_{ef}\frac{\partial u_j}{\partial x_i}\right)$
Thermal energy	T	$\alpha_{ef} = \frac{\nu}{Pr} + \frac{\nu_t}{Pr_t}$	0
Turbulent kinetic energy	k	$\nu + \frac{\nu_t}{\sigma_k}$	$P_k + G_k - \tilde{\varepsilon} + D_k$
Dissipation rate of k	$\tilde{\varepsilon}$[a]	$\nu + \frac{\nu_t}{\sigma_\varepsilon}$	$\frac{\tilde{\varepsilon}}{k}(f_1 C_{\varepsilon_1} P_k - f_2 C_{\varepsilon_2}\tilde{\varepsilon} + C_{\varepsilon_1} C_{\varepsilon_3} G_k) + E_\varepsilon$

$P_k = \nu_t\left(\frac{\partial u_i}{\partial x_j} + \frac{\partial u_j}{\partial x_i}\right)\frac{\partial u_i}{\partial x_j}$; $G_k = g_j\beta\frac{\nu_t}{Pr_t}\frac{\partial T}{\partial x_j}$

[a] $\tilde{\varepsilon} = \varepsilon + D_k$ is adopted as the "dissipation variable" for the computational convenience of specifying its value at the walls as zero.

Table 2
The low-Re k–ε turbulence model of Nagano and Hishida [21]: constants, wall-boundary conditions (BC) for k and $\tilde{\varepsilon}$; modification functions (f) and extra-terms (D_k, E_ε)

C_{ε_1}	C_{ε_2}	σ_k	σ_ε	k_w – BC	$\tilde{\varepsilon}_w$ – BC
1.45	1.9	1.0	1.3	0	0
f_μ	f_1	f_2	D_k	E_ε	
$\left[1-\exp\left(\frac{-x_n^+}{26.5}\right)\right]^2$	1	$1-0.3\exp(-Re_t^2)$	$-2\nu\left(\frac{\partial\sqrt{k}}{\partial x_j}\right)^2$	$\nu\nu_t(1-f_\mu)\left(\frac{\partial^2 u_i}{\partial x_j \partial x_k}\right)^2$	

convective fluxes at each face of the control volumes were approached with the hybrid central/upwind difference scheme. Velocities and pressures were calculated by the SIMPLEC algorithm with the enhancements recommended in Ref. [25], and the discretized equations were solved by a tri-diagonal matrix algorithm. After grid-dependence tests [19], a 70×70 non-uniform staggered grid was used for the present calculations. The criteria for convergence of the iterative calculation, to be simultaneously satisfied, were: (i) normalised sum of the absolute residuals for the discretized equations $\leq 5 \times 10^{-5}$; (ii) maximum normalised iterative change $\leq 5 \times 10^{-5}$ for all variables; (iii) relative iterative change of the outlet temperature $\leq 0.01\%$ and (iv) overall energy balance satisfied to within 0.05% of the thermal energy conveyed into the cavity by the jets.

By exploratory calculations [19], it was verified that, for levels of $I_{t_{in}} < 10\%$, the flow field solutions were rather insensitive to the assumed distributions and precise values of k and $\tilde{\varepsilon}$ at the inlet sections. In fact, the transport equations of these variables are source-term dominated, and the global level of turbulence intensity in the recirculating flow domain is mainly established by the strong shear production of k in the early mixing layer of the jets. In contrast, the shape of the streamwise velocity inlet profiles was observed to significantly affect the growth of the jets and the local wall heat transfer rate up to a distance of 25–30 slot widths. Thus, in all calculations, uniform profiles were assumed for k and $\tilde{\varepsilon}$ (as well as for T) at the jet inlet sections, with the values:

$$k_{in} = 1.5\, I_{t_{in}}^2 U_c^2 \tag{6}$$

$$\tilde{\varepsilon}_{in} = k_{in}^{3/2}/L_\varepsilon \tag{7}$$

respectively, where L_ε is a length scale for dissipation, taken here as $d_j/2$, and an average value of $I_{t_{in}} = 4\%$ was assigned for both jets. Since a wide range of jet flow rates was to be considered, either a parabolic or a logarithmic (or mixed, with gradual transition) channel flow profile was specified for the streamwise mean velocity component, according to the value of each jet Reynolds number. At the outlet section, zero normal gradients were specified for all variables, except for u, which was iteratively corrected to ensure overall mass balance (see Ref. [19] for details). The temperature value was specified on the isothermal solid walls, where the no-slip condition was assumed for velocity.

3. Results and discussion

3.1. Flow reversal

In the course of laboratory experiments carried out with the same experimental set-up described in Ref. [19], important disturbances were observed in the structure of the recirculating flow, which were mainly due to the dominant effect of the downward buoyancy forces at the entry region of the horizontal jet. Specifically, a complete flow reversal was verified for the parameter configuration defined by: $L/H = 1$ ($H = 1.04$ m), $d/H = 0.019$, $Re_g = 373$ ($U_c = 0.14$ m/s), $Re_h/Re_v = 1.8$, $Fr_h = 1.7$ and $\Theta_w = 0.53$ [26,27]. The corresponding flow and temperature fields calculated with the present methodology are illustrated in Fig. 2. They are characterised by the inversion of the normally clockwise circulation of the main vortex, which is imposed by the downfall of the incoming cold air (horizontal jet) along the left side wall. Consequently, the upcoming warm jet is prematurely separated from the wall and deflected to the right. As it will be referred again later, the numerical predictions indicate that such occurrence may be critical for the thermal comfort in room ventilation, since the maximum velocity in the lower part of the compartment (generally represented by U_{rm}) almost doubles with respect to a clockwise circulation flow pattern at a similar ventilation rate ($U_{rm} = 0.88U_c$ against $0.46U_c$, respectively — cf. Fig. 2(d) with Figs. 5(b) and 8(b) in Ref. [19]). In fact, in a normal clockwise-rotating flow pattern, the flow associated with U_{rm} is fed by the recirculation itself. However, with flow reversal, it is further reinforced by the (cumulative) warm and cold air incoming flows, as it is apparent from Fig. 2(a).

The particular conditions that may lead to the flow reversal come out as a result of the parametric study presented in the next section.

3.2. Parametric study

For optimisation purposes in the scope of thermal comfort, systematic calculations were conducted to assess the

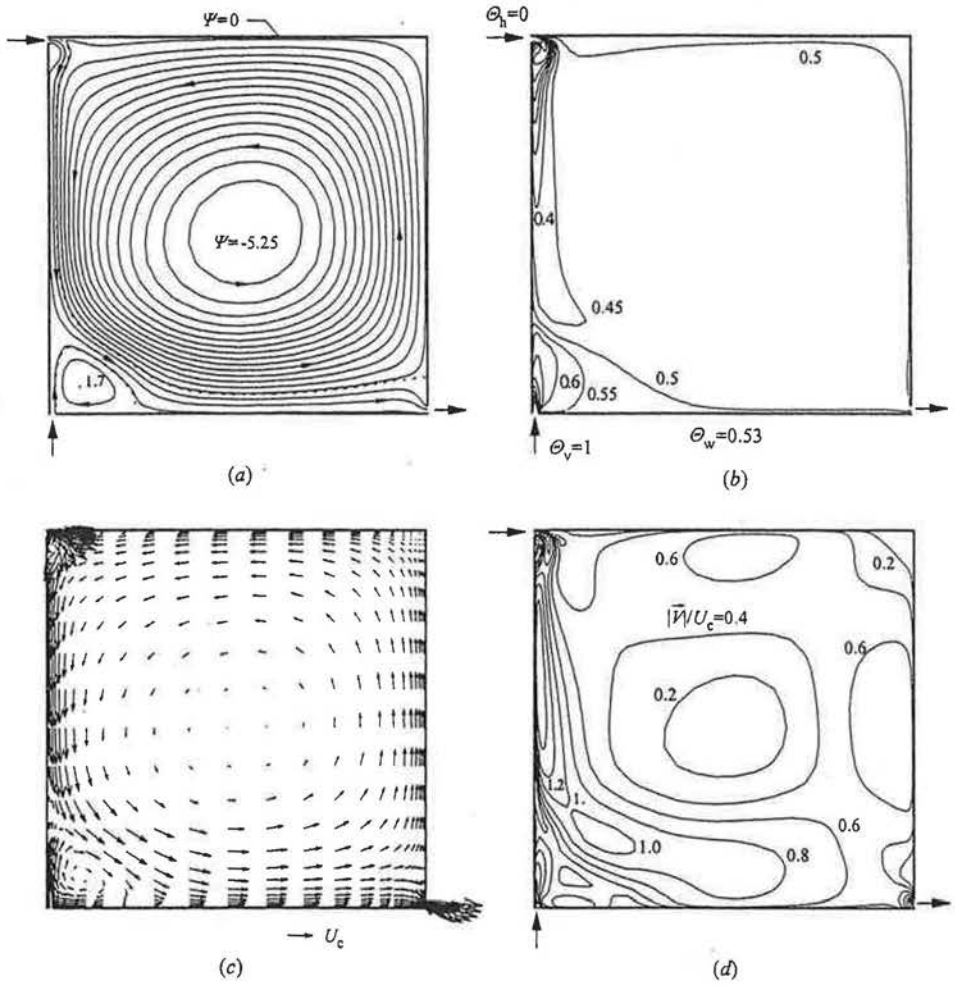

Fig. 2. Predicted flow reversal for the parametric configuration quoted in Refs. [26,27]: (a) streamline pattern ($\Delta\Psi = 0.345$), (b) isotherms ($\Delta\Theta = 0.05$), (c) velocity vectors and (d) lines of isovalues of the velocity modulus. ($H = 1.04$ m, $U_c = 0.14$ m/s.).

influence of the different geometric, dynamical and thermal parameters on the flow and heat transfer characteristics in a room with a mixing flow heating–ventilation system, such as the one sketched in Fig. 1. The ranges of parameter values covered by the calculations are given in Table 3.

Characterising a balance between the inertia and the viscous forces, a global (air supply) Reynolds number is here defined as $Re_g = U_c L_c/\nu$, where U_c and L_c are characteristic velocity and length scales of the incoming forced flow, respectively, expressed by $U_c = (U_h d_h + U_v d_v)/(d_h + d_v)$ and $L_c = d_h + d_v$. Consequently, $Re_g = Re_h + Re_v$ under the Boussinesq approximation, and $U_c = (U_h + U_v)/2$ if $d_h = d_v = d$, as considered in the course of the present study. Being directly proportional to the supply airflow rate, Re_g is likewise proportional to the air exchange rate for a given room geometry. In practical problems of room ventilation, this parameter is usually expressed by the *number of air changes per hour*, N_{ac}, which can be written as:

$$N_{ac} = 3600\nu\frac{Re_g}{HL}[\mathrm{h}^{-1}] \tag{8}$$

if both jets are assumed to contribute for the air renewal. In turn, the balance between buoyancy and inertia forces may be represented by a global Archimedes number Ar_g [$= (Gr_H/Re_g^2)\cdot(L_c/H)^2$, cf. Nomenclature] or, locally in each inlet region, by the respective jet Froude number $Fr_j\{= U_j/[g\beta d_j(T_v - T_h)]^{1/2},\ j = 1,2\}$.

For every study of a parameter influence, Re_g was made to vary approximately between 10^{-1} and 10^5 (Ar_g

Table 3
Scheme of the parametric study, for the configuration of Fig. 1. Fixed parameters: $H = 3$ m, $T_v - T_h = 25$°C and $d_h = d_v = d$. The same temperature value is assigned to all the four walls

Influence of:	L/H	d/H	Θ_w	Re_h/Re_v	Re_g
L/H	**1–4**	0.02	0.25; 0.5	1	10^{-1}–10^5
d/H	3	**0.01–0.1**	0.25	1	10^{-1}–10^5
Θ_w	3	0.02	**0–0.5**	1	10^{-1}–10^5
Re_h/Re_v	3	0.02	0.25	**0.25–10**	10^{-1}–10^5
			0.5	**0.5–2**	

$\approx 10^{9}$–10^{-3}) ranging from purely buoyant to forced flow regimes, through a mixed convection zone where the flow may be unstable due to the conflict between the two natures of forces. To set the numerical results free from any "hysteresis" effects, which naturally occur when approximate solutions of the relevant variables are taken as initial guesses [4], every iterative calculation was started with the following initial field distributions: zero-velocity, uniform temperature at some level between T_h and T_v, and k and $\tilde{\varepsilon}$ were initialised with the average of the respective values at the jet inlets.

The results of the parametric study will now be exposed and discussed.

3.2.1. Room geometry

The influence of the room aspect ratio on the flow characteristics was studied for values of L/H between 1 and 4, taking $d/H = 0.02$ and $Re_h/Re_v = 1$ (i.e., equal ventilation and heating airflow rates), and two wall-temperature levels: $\Theta_w = 0.25$ and 0.5. For each of these cases, Fig. 3(a) and (b) shows the variation of the *maximum velocity in the return flow*, U_{rm}, as a function of N_{ac}. It is seen that, for a given air exchange rate, U_{rm} is not significantly affected by the room aspect ratio, particularly for $L/H \geq 2$. The results with $L/H = 1$ [omitted in Fig. 3(a)] present lower values of U_{rm} for $N_{ac} \geq 50\ h^{-1}$ [1] and, for $\Theta = 0.5$, they show discontinuities in the range $1 < N_{ac} < 10\ h^{-1}$, that are associated to the occurrence of the flow reversal, as described previously. In these cases, it was observed that the flow pattern is rather similar to that of the configuration represented in Fig. 2, where $Re_h/Re_v = 1.8$.

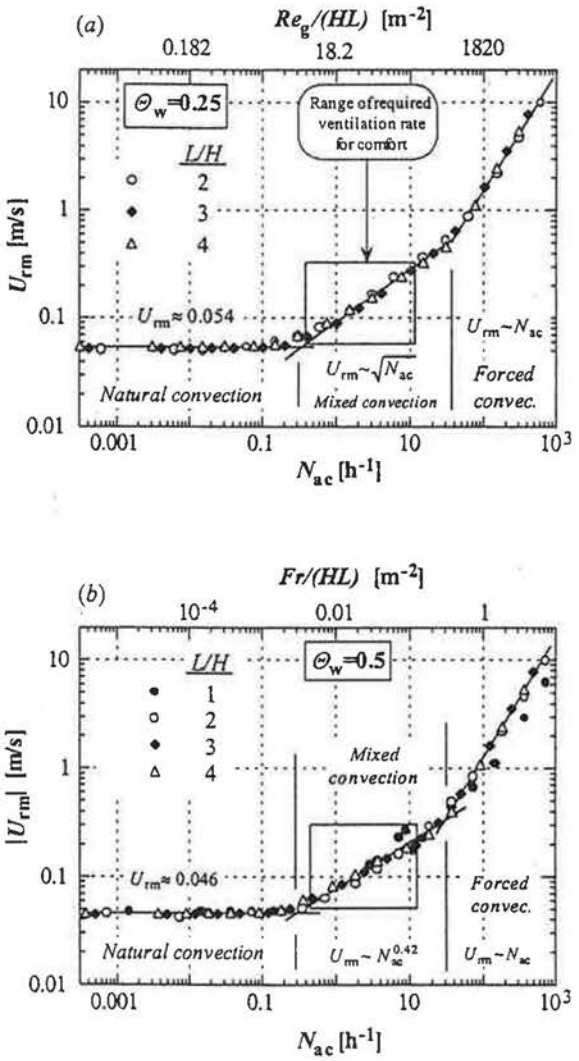

Fig. 3. Influence of L/H on the maximum velocity in the return flow U_{rm}, as a function of the number of air changes per hour N_{ac}: (a) $\Theta_w = 0.25$ and (b) $\Theta_w = 0.5$. (——): Curves fitted to the set of results obtained with $L/H = 2$, 3 and 4. ($d/H = 0.02$ and $Re_h/Re_v = 1$.).

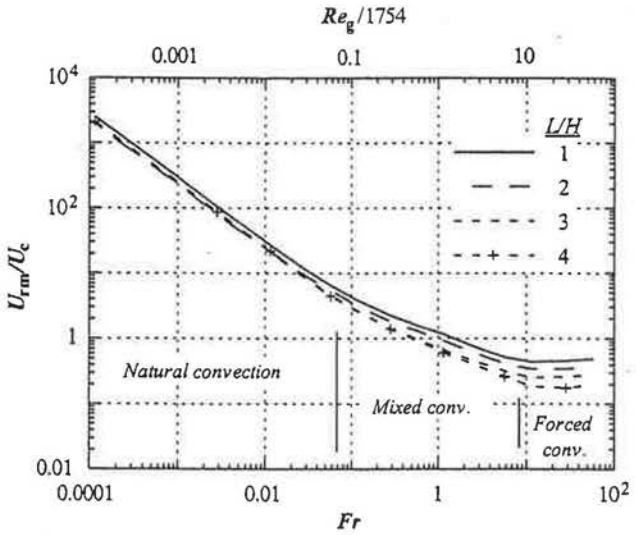

Fig. 4. Relation between U_{rm} and characteristic (average supply air) velocity U_c, as a function of $Fr(= Fr_h = Fr_v)$ and of Re_g. ($\Theta_w = 0.25$, $d/H = 0.02$ and $Re_h/Re_v = 1$.).

Three distinct zones are apparent in these figures, corresponding to three flow regimes: (i) a *natural convection* flow regime, below $N_{ac} \approx 0.1$–0.3, where U_{rm} remains constant, thus unaffected by the increasing momentum of the jets, because the recirculating flow is primarily promoted by the buoyancy forces that accelerate the incoming warm airflow of the vertical jet; (ii) a *mixed convection* regime up to $N_{ac} \approx 30\ h^{-1}$, where the inertia and the buoyancy forces are globally of the same order of magnitude, and U_{rm} grows approximately as $N_{ac}^{1/2}$ [or as $U_c^{1/2}$, for a fixed room geometry, cf. Eq. (8)]; (iii) finally, a *forced convection* regime with a linear dependence of U_{rm} on N_{ac}, where the flow pattern is nearly independent of the

[1] Such lower values of U_{rm} are probably due to the effects of numerical diffusion, which prevail in the regions where the flow is not aligned with the Cartesian grid directions. As L/H grows, the extension of such regions loses importance relatively to the whole calculation domain.

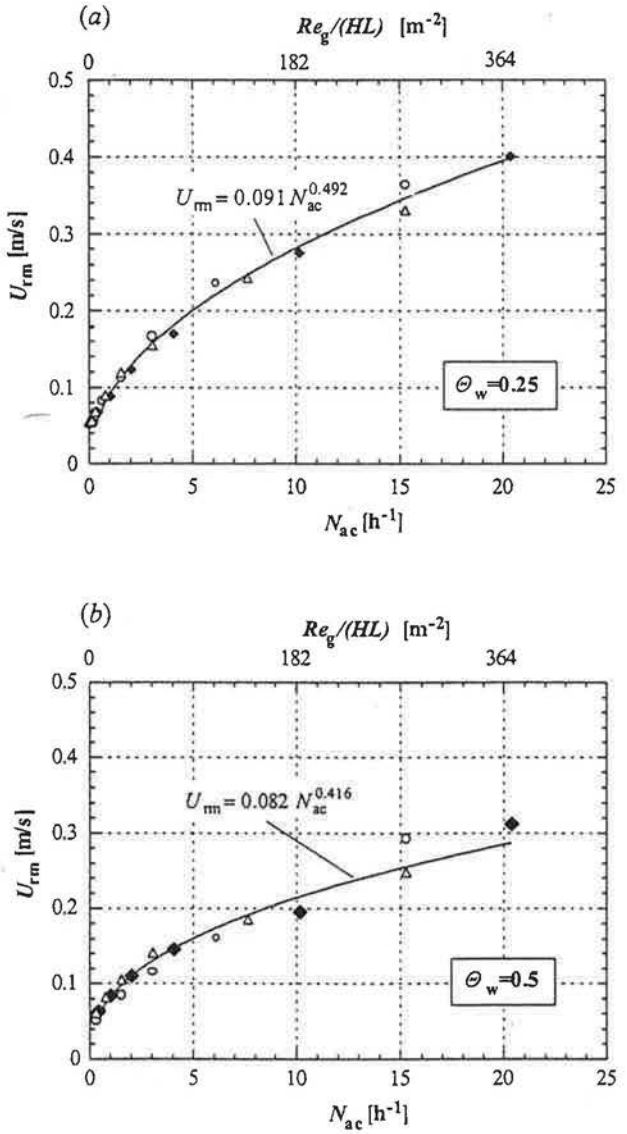

Fig. 5. Variation of the maximum velocity in the return flow in the mixed convection regime for $L/H \geq 2$: (a) $\Theta_w = 0.25$ and (b) $\Theta_w = 0.5$. (Symbols with the same meaning as in Fig. 3; $d/H = 0.02$ and $Re_h/Re_v = 1$.).

Reynolds number (self-similar flow) and U_{rm}/U_c (or U_{rm}/Re_g) is almost constant for each L/H (cf. Eqs. (1a), (1b) and (1c)).

The relations Re_g/HL and Fr/HL — proportional to N_{ac} — are labelled in the upper axis of Fig. 3(a) and (b), for easier reference to the non-dimensional parameters (note that $Fr_h = Fr_v = Fr$ when $Re_h/Re_v = 1$). Thus, it may be said that the zones corresponding to the mixed convection regime are naturally centred on the values of the jet Froude number Fr close to unity. This is more apparent in the non-dimensional representation of Fig. 4, which allows to conclude that, for $Fr \approx 1$ (and verified for all studied values of Θ_w), U_{rm} is close to the values of the supply air average velocity (i.e., $U_{rm}/U_c \approx 1$). Besides, Fig. 4 shows clearly the regime of self-similarity of the flow, starting at about $Re_g \geq 1.5 \times 10^4$ ($Fr \geq 8.5$), for any L/H. This value of Re_g corresponds to jet Reynolds numbers of $Re_j \geq 7500$, which is close to the values referred by other authors for different one-jet configurations: e.g., $Re_j \approx 5000$–8000 [4] and $Re_j \approx 8100$ [28].

By Fig. 3(a) and (b), it may also be inferred that the most common values of room ventilation requirements in non-industrial buildings — generally, N_{ac} between 0.3 and 5–10 h^{-1} [29,30] — lie in the mixed convection flow regime, thus emphasising the importance of a reliable assessment of heat transfer for the numerical prediction of such low-turbulence flows. The details of the box-limited zones in Fig. 3(a) and (b) are represented in Fig. 5(a) and (b), respectively, where the best fits found for the $U_{rm} \sim N_{ac}$ relations are plotted in linear coordinates. A comparison of these latter allows to better quantify the influence of the wall-temperature level Θ_w on the maximum velocity in the occupied zone: for example, when $\Theta_w = 0.25$, the value $U_{rm} = 0.2$ m/s — usually taken as the limit level for thermal comfort — is reached with five air changes per hour, while $N_{ac} = 8.5$ h^{-1} will be needed, when $\Theta_w = 0.5$. The opposing effect on U_{rm} of an increasing Θ_w, in the natural and mixed convection regimes, is related to the decrease of the assisting buoyancy forces acting on the vertical (warm) jet, since the temperature level of the internal ambient increases with Θ_w.

It was verified that, within the range of velocity values with practical interest, the central region of the compartment remains practically isothermal, as expected for a mixing flow ventilation system. Therefore, the temperature at the centre Θ_c may be taken as representative of the ambient temperature level in the occupied zone. Thus, from Fig. 6, it can be predicted that, keeping $\Theta_w = 0.25$ and $Re_h/Re_v = 1$, the effective heating of the room will

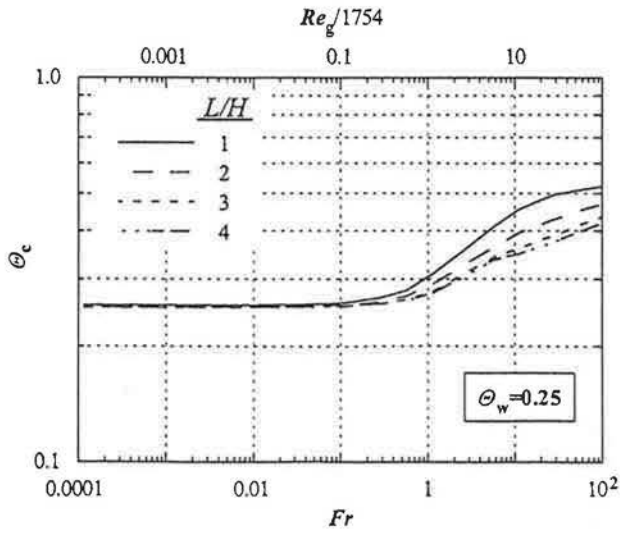

Fig. 6. Variation of the temperature at the center Θ_c with the flow regime for different values of L/H. ($d/H = 0.02$ and $Re_h/Re_v = 1$.).

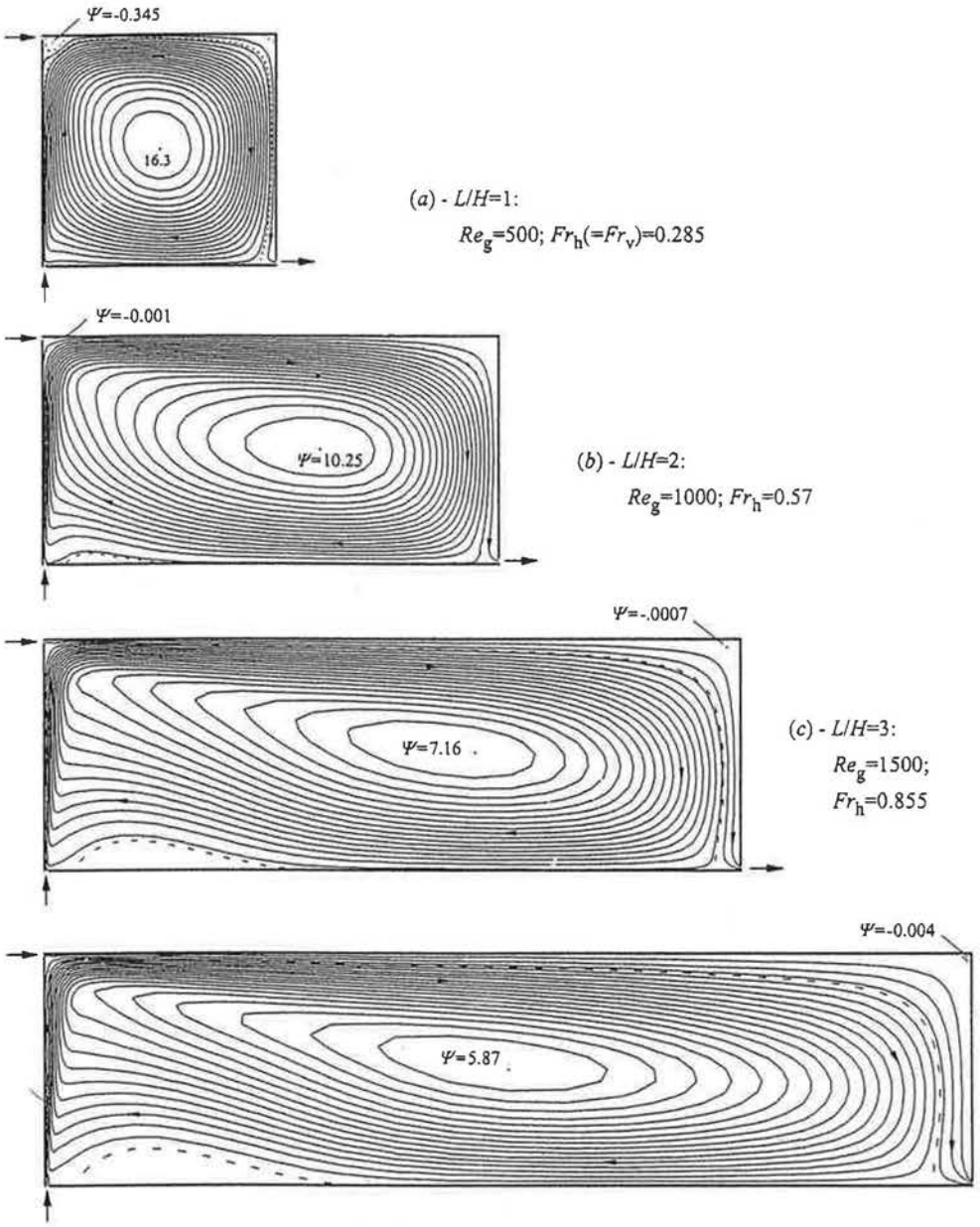

Fig. 7. Streamline patterns for different room geometries, with $L/H = 1$–4, for the same air exchange rate: $N_{ac} = 3.05\ h^{-1}$. ($d/H = 0.02$, $\Theta_w = 0.25$ and $Re_h/Re_v = 1$.).

be accomplished only for $Fr > 1$ ($Re_g > 1750$, approximately) and, as expected, more difficult to achieve as L/H increases.

The following figures illustrate some relevant aspects of the influence of the room geometry on the flow structure. The predicted streamline patterns at a fixed air exchange rate of $N_{ac} = 3.05\ h^{-1}$ are represented in Fig. 7(a)–(d), for increasing values of the room aspect ratio L/H between 1 and 4. In any of these configurations, the flow field is essentially characterised by the main clockwise recirculation, which determines the airflow rate sweeping the lower part of the occupied zone and, consequently, the value of U_{rm}. The secondary, counter-clockwise recirculation associated with the separation of the return flow from the left part of the bottom wall, as shown in Fig. 7(b)–(d), is a characteristic of the mixed convection flow regime.[2] It represents a poorly ventilated zone that is wider for higher L/H. In spite of the different geometries, the sequence from (a) to (d) in Fig. 7 illustrates the changes that could

[2] This detail was exclusively observed for values of the jet Froude number in the range $0.1 < Fr < 10$, irrespective of L/H (≥ 2) and of d/H.

normally be observed in the flow of the horizontal jet when its discharge velocity is gradually increased. [Note that, for fixed H and N_{ac}, Re_g (as well as Fr_h) increase directly with L/H (cf. Eq. (8))]. In Fig. 7(a) ($Fr_h = 0.285$), it is seen that, due to the adverse buoyancy forces, the horizontal (cold) jet falls down as it enters the room, which is a characteristic of the whole regime of natural convection. However, the corresponding zone of separated flow remains very restricted by the upcoming flow of the vertical (warm) jet, which was meanwhile accelerated by the assisting buoyancy forces. This is also the case in Fig. 7(b) ($Fr_h = 0.57$), where the separation of the cold jet from the adjacent wall is very slight and just indicated by the negative (and minimum) value of the stream function. In Fig. 7(c) and (d), such separation is no longer observed. From the present predictions, it could be stated that, for values of Fr_h greater than unity, inertia becomes dominant over buoyancy in the domain of the cold jet, which then remains definitively attached to the top wall. In particular for $L/H = 3$, it was verified that the *critical* Froude number (in this sense) was $Fr_{h_{cr}} \approx 0.53$.

The just described details of the flow are more clearly identified with the three flow regimes in Fig. 8, for a room aspect ratio of $L/H = 3$: (a) natural, (b) mixed and (c) forced convection regimes. As will be seen in Section 3.2.3, under more critical conditions regarding the conflict between inertia and buoyancy forces (e.g., for $Re_h/Re_v > 1$ and $\Theta_w \geq 0.25$), important modifications of the flow pat-

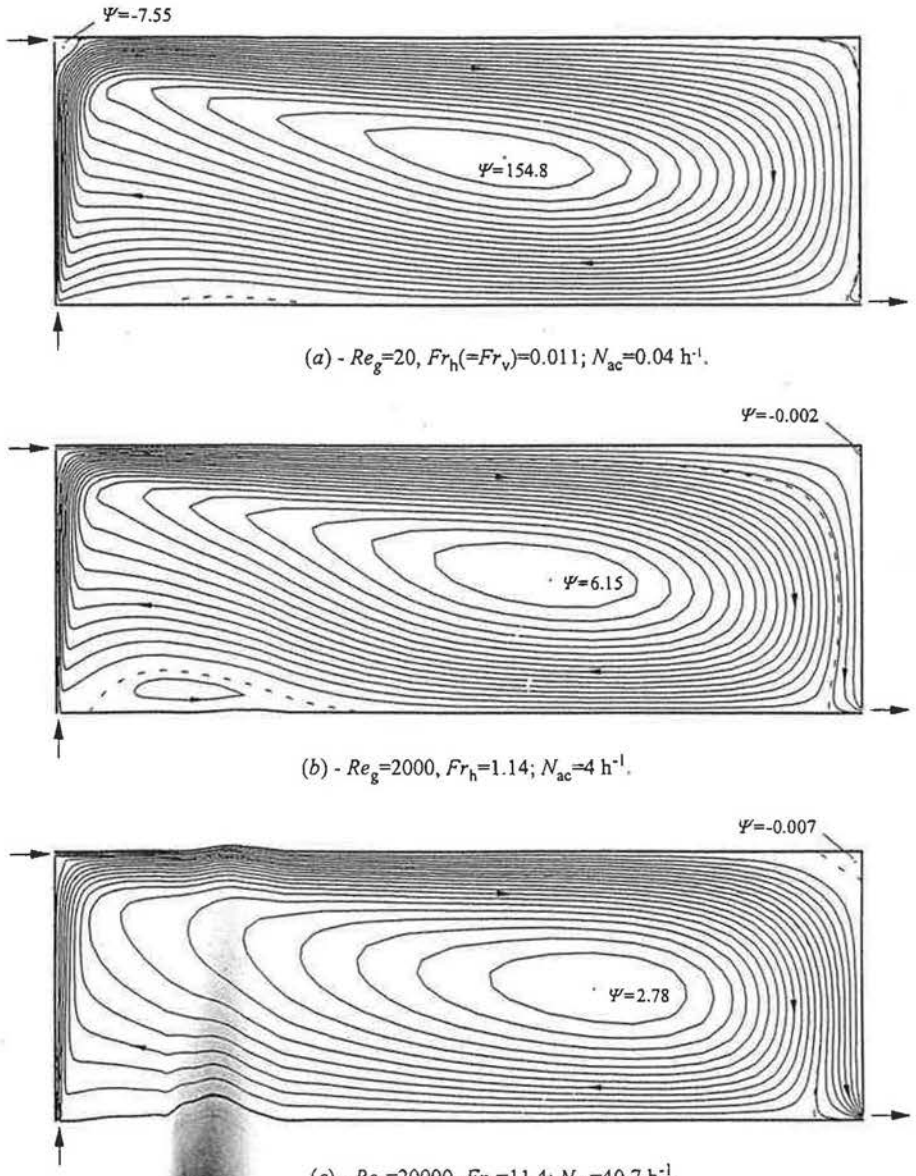

Fig. 8. Flow patterns that are typical of the [illegible]vection regimes, for $\Theta_w = 0.25$ and $Re_h/Re_v = 1$: (a) natural, (b) mixed and (c) forced convection. ($L/H = 3$, $d/H = 0.02$.).

tern may occur in the mixed convection regime, including the complete flow reversal with a variety of transitional, complex flow structures.

For the mixed convection configuration of Fig. 8(b) (i.e., $Re_g = 2000$, $N_{ac} = 4\ h^{-1}$), the predicted isoline distributions of (a) the velocity modulus, (b) the turbulent viscosity and (c) the turbulence intensity are graphically represented in Fig. 9, where the occupied zone of the room is delimited by a dashed line (cf. definition in Ref. [31]). Apart from the outlet region, the higher velocity values are registered in the domains of the vertical jet ($|\vec{V}|/U_c = 2.3$, at $y/H = 0.12$) and of the horizontal jet ($|\vec{V}|/U_c = 1.56$, at $x/L = 0.086$), thus outside the occupied zone. Within it, the maximum velocity is $U_{rm} = 0.66U_c$, at the level $y/H = 0.073$ in the return flow — a value that complies with the recommended air velocity limits for thermal comfort (cf. Ref. [32]). Fig. 9(b) shows that the flow in the lower left region of the compartment remains practically laminar. This feature is also common to the whole natural convection regime, where the level and the distribution of ν_t are nearly independent of Re_g. On the contrary, in the forced convection regime, the numerical results showed that the turbulence level tends to significantly increase with the supply airflow rate, and the whole flow field remains frankly turbulent. Fig. 9(c) indicates that the occupied zone is characterised by low levels of the turbulence intensity ($I_t \leq 20\%$), which increase towards the outlet side of the room. The higher values of I_t are registered in the free-mixing layers of the horizontal jet ($\approx 45\%$) and of the vertical jet ($\approx 40\%$), nearly at the locations where they are hit by the upcoming warm airflow and by the return flow, respectively.

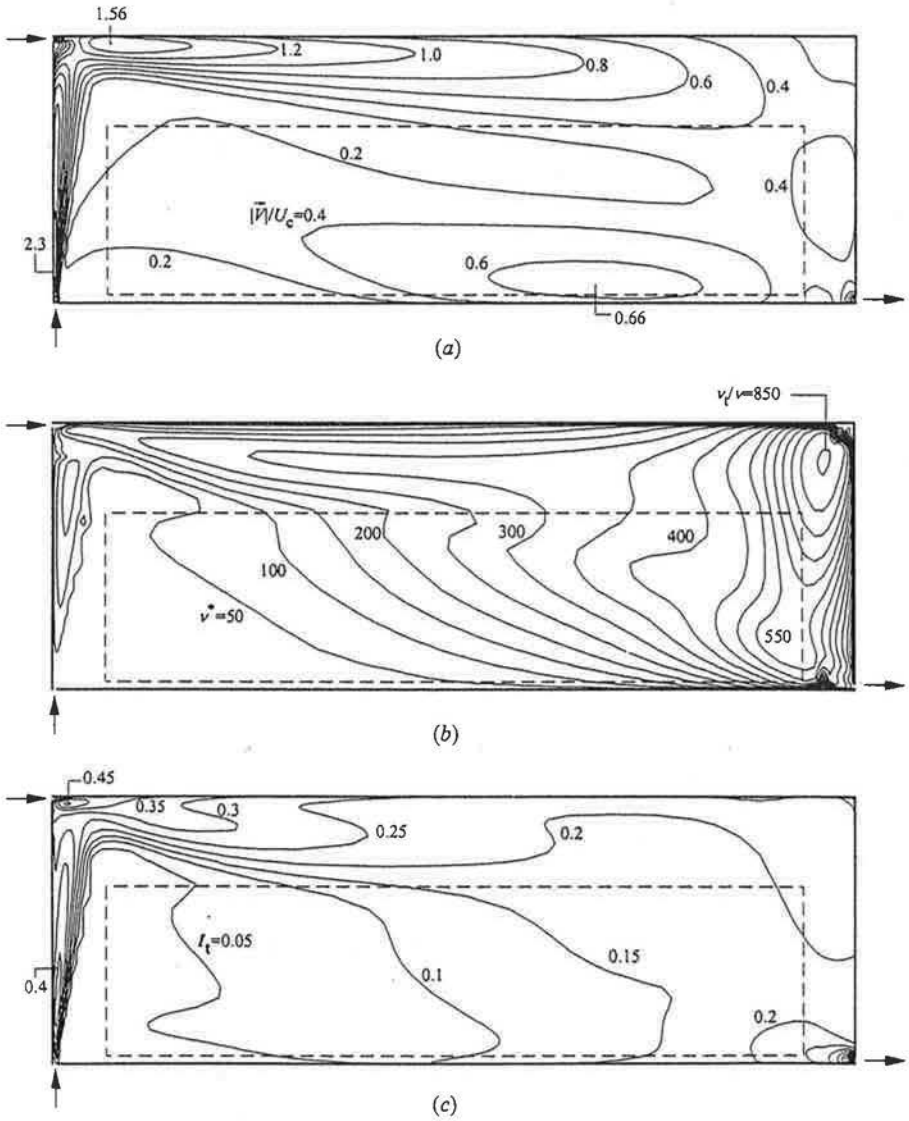

Fig. 9. Lines of isovalues of the non-dimensional (a) velocity modulus, $|\vec{V}|/U_c$, (b) turbulent viscosity, $\nu^* = \nu_t/\nu$, and (c) turbulence intensity, I_t, for the mixed convection configuration of Fig. 8(b): $Re_g = 2000$, $Fr_h = 1.14$; $N_{ac} = 4\ h^{-1}$, $U_c = 0.258$ m/s. (– – – –): Limits of the *occupied zone*.

3.2.2. Width of the jet inlet sections

The width of jet inlet sections was made to vary within the range $d/H = 0.01$–0.1, keeping $d_h = d_v = d$ and the remaining conditions as quoted in Table 3. Fig. 10(a) and (b) show the influence of d/H on U_{rm}/U_c, for $Re_g(H/d) = 4 \times 10^4$ and 2×10^5, respectively (i.e., corresponding to $U_c \approx 0.1$ and 0.5 m/s). The right and the upper axis provide a direct relation between N_{ac} and U_{rm}. It may be directly inferred that, *for a fixed supply air velocity* in a compartment with a given geometry, the maximum velocity in the return flow varies approximately as $(d/H)^{1/2}$.

Generally, the determining parameter is the required ventilation rate for a certain application. In Fig. 11(a), the variations of U_{rm}/U_c with d/H are plotted *for specific values of the supply airflow rate* — i.e., for fixed values of Re_g or of the air exchange rate, N_{ac}, if the room geometry (L/H) is the same. Thus, it may be concluded that, for the higher flow regimes, U_{rm}/U_c increases linearly with d/H,

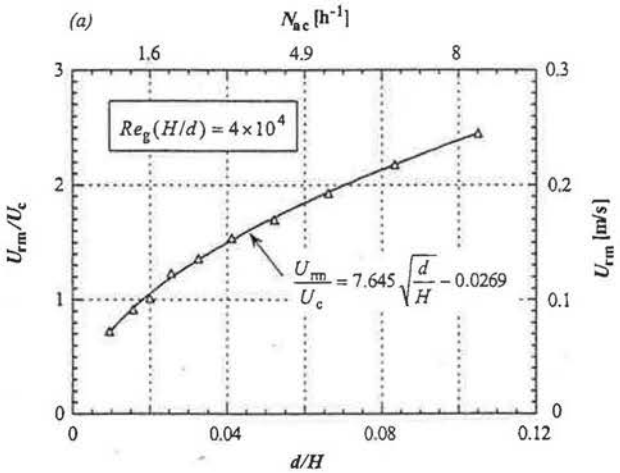

Fig. 10. Influence of d/H on the maximum velocity in the return flow, for fixed values of the supply air velocity: (a) $U_c \approx 0.1$ m/s and (b) $U_c \approx 0.5$ m/s. ($L/H = 3$, $\Theta_w = 0.25$ and $Re_h/Re_v = 1$.).

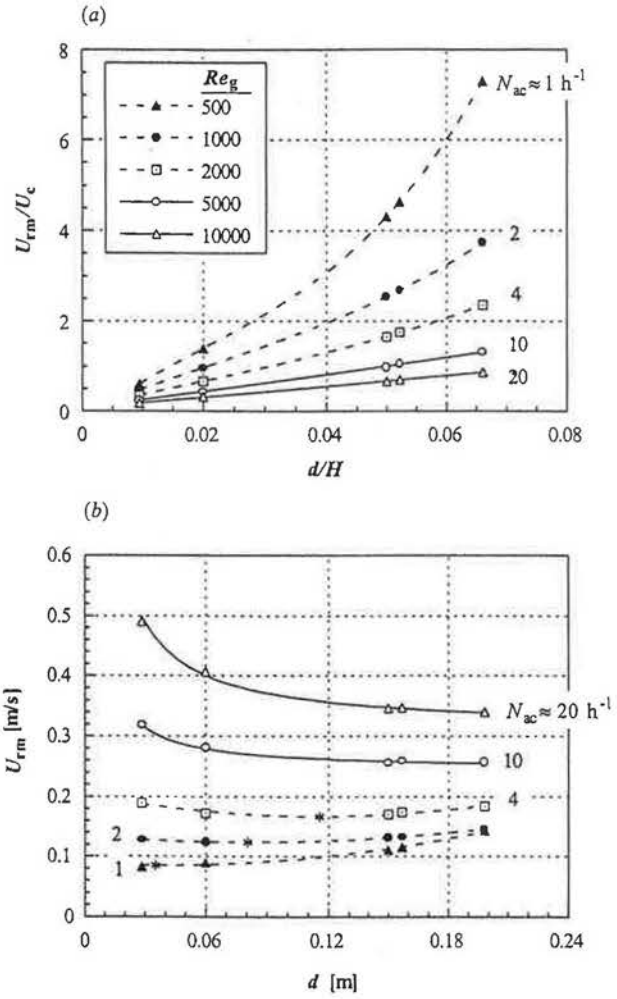

Fig. 11. (a) Dimensionless and (b) dimensional representation of the dependence of U_{rm} on the jet slot width, d, for different values of Re_g (i.e., of the supply airflow rate) in the mixed convection flow regime. [$L/H = 3$, $\Theta_w = 0.25$ and $Re_h/Re_v = 1$; $H = 3$ m. (*): Locations of the probable minima of U_{rm}.].

a variation that becomes less uniform and more accentuated for lower ventilation rates ($N_{ac} \leq 4$ h^{-1}, $Re_g \leq 2000$).

The inference from Fig. 11(a) of the absolute values of U_{rm} for practical purposes is somewhat difficult, since U_c varies inversely with d/H, *when Re_g is kept constant.* Alternatively, Fig. 11(b) illustrates the corresponding dimensional relations $U_{rm} \sim d$, allowing to conclude that: (i) for higher levels of the supply airflow rate ($N_{ac} \geq 10$ h^{-1}, and constant), U_{rm} varies inversely with d, according to relations like:

$$U_{rm} = 0.244 + 2.064 \times 10^{-3} d^{-1}\,[\mathrm{m}], \quad \text{for } N_{ac} = 10\,\mathrm{h}^{-1} \tag{9a}$$

or

$$U_{rm} = 0.312 + 5.30 \times 10^{-3} d^{-1}\,[\mathrm{m}], \quad \text{for } N_{ac} = 20\,\mathrm{h}^{-1} \tag{9b}$$

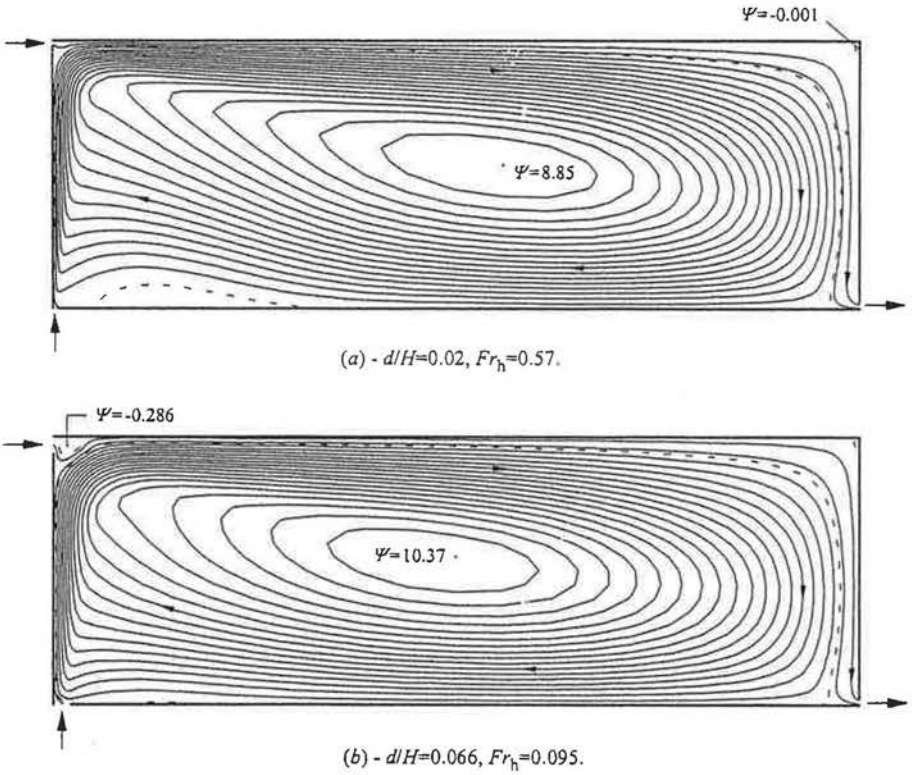

Fig. 12. Streamline patterns for $Re_g = 1000$ ($N_{ac} \approx 2\ h^{-1}$): (a) $d/H = 0.02$ and (b) $d/H = 0.066$. ($L/H = 3$, $\Theta_w = 0.25$ and $Re_h/Re_v = 1$; $H = 3$ m.).

In such cases, the flow field is essentially dominated by inertia and the variation of U_{rm} with an increasing d is mainly determined by the inherent decrease of the initial momentum of the jets. (ii) For lower air exchange rates ($N_{ac} \leq 4\ h^{-1}$ in the figure), that are more common to room ventilation problems, the variations of U_{rm} present minima within the studied range of d, which might, in this sense, correspond to optimal values of d and are marked by an asterisk in Fig. 11(b): $d_{opt} = 3.6$, 8.1 and 11.6 cm, for $N_{ac} = 1$, 2 and 4 h^{-1}, respectively. The corresponding fitted curves (dashed lines) are thus divided into two branches. When $d < d_{opt}$, the variation of U_{rm} is still typical of the forced flow regime, as explained above in (i). For constant Re_g, higher jet slot widths imply lower initial momentum of the jets and, as d increases above d_{opt}, the flow field becomes gradually more dominated by the buoyancy forces. These forces act mainly in the domain of the vertical jet flow (which is wider as d grows), by accelerating it, thus promoting the increase of the rate of recirculating airflow and, therefore, of the return flow associated with U_{rm}.

In Fig. 12, a comparison is made of the flow fields calculated for $Re_g = 1000$ ($N_{ac} \approx 2\ h^{-1}$), considering two different values of the jet slot widths, (a) $d/H = 0.02$ and (b) 0.066, lying each from either side of d_{opt} on the corresponding curve in Fig. 11(b) (i.e., $d = 0.06$ and 0.198 m, respectively). It is seen that the total return airflow rate — represented, in dimensionless terms, by $(\Psi_{max} - 1)^3$ — is clearly greater in the latter case: 9.37 against 7.85.[4] Fig. 12 shows also the different evolutions of the horizontal cold jet: in (a), it remains attached to the ceiling (inertia dominated), while in (b), it "falls down" prematurely, as it is typical in the natural convection flow regime (buoyancy-dominated).

Thus, one might say that each minimum of U_{rm} marked in Fig. 11(b) approximately represents the conditions for transition between the domains of predominance of the buoyancy and the inertia forces, for the respective value of Re_g (or of N_{ac}). Such *critical* conditions are plotted in Fig. 13 as a function of d/H, for a room geometry of $L/H = 3$; however, Fig. 3(a) suggests that they should be applicable to any value of L/H between 1 and 4, under the same remaining parameters. It should be remarked that the linear relation $Re_{g_{cr}} \sim d/H$ (or $N_{ac_{cr}} \sim d$) shown in Fig. 13 is equivalent, by the definition of Re_g, to a "critical" value of the mean jet discharge velocity, that is almost indepen-

[3] The subtractive value $\Psi = 1$ [dashed lines in Fig. 12(a) and (b)] means the cumulative airflow rate of both jets (see the definition of Ψ), which is equal to the exhaust airflow rate.

[4] For $Re_g = 500$ ($N_{ac} \approx 1\ h^{-1}$), the difference is much more notorious (cf. the values of U_{rm} on the corresponding curve in Fig. 11(b)): $\Psi_r = 11.9$ and 18.5, for $d = 0.06$ and 0.198 m, respectively.

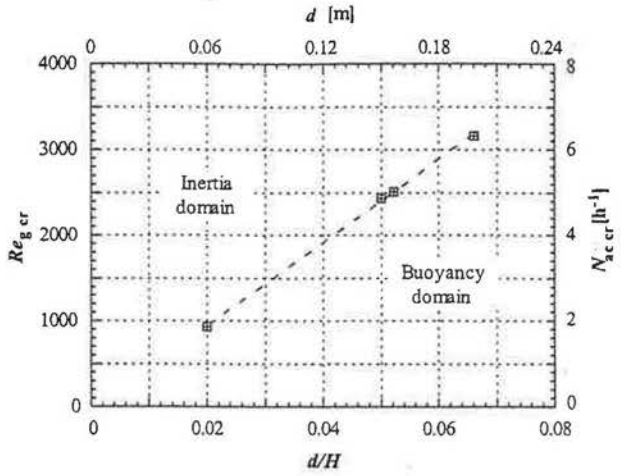

Fig. 13. Critical Re_g (and N_{ac}) as a function of the jet slot widths, stating a transition between the domains of forced and natural convection, in the horizontal jet flow development. ($L/H = 3$, $\Theta_w = 0.25$ and $Re_h/Re_v = 1$; $H = 3$ m.).

dent of d/H, but will certainly depend on other parameters that were kept constant in the present study (e.g., Θ_w, Re_h/Re_v, $\Delta\Theta_v$, or even H). Such value may be called *optimum* in the sense that it is related with a minimum U_{rm}, and it reads $U_{c_{opt}} \approx 0.13$ m/s when $H = 3$ m.

3.2.3. Ratio between the ventilation and heating airflow rates. Temperature of the walls

In this section, an analysis is made of the effects of varying the ratio between the horizontal and the vertical jet Reynolds numbers and the temperature of the walls. It is shown that these are the parameters that, under certain combined conditions, determine the occurrence of drastic modifications of the flow structure, namely the complete flow reversal. Considering a compartment with $L/H = 3$, and $d/H = 0.02$ for both jets, the ratio Re_h/Re_v was made to vary between 0.25 and 10, for $\Theta_w = 0.25$, and from 0.5 to 2, for $\Theta_w = 0.5$ (cf. Table 3). In any case, the range $Re_g = 10^{-1}$–10^5 was covered, while Θ_w is taken uniform and equal for all the walls.

In agreement with the conclusions drawn in Section 3.2.1, after the comparative analysis of Fig. 5(a) and (b), the results plotted in Fig. 14 show that, as the level of Θ_w is increased, the maximum velocity in the return flow tends to decrease, mainly in the natural and mixed convection flow regimes. Such effects derive essentially from the decreasing importance of the (normally assisting) buoyancy forces acting in the domain of the vertical jet.

It was already referred, with respect to Fig. 3(b) ($Re_h/Re_v = 1$, $\Theta_w = 0.5$, $L/H = 1$), that a higher temperature of the walls promoted the occurrence of *flow rever-*

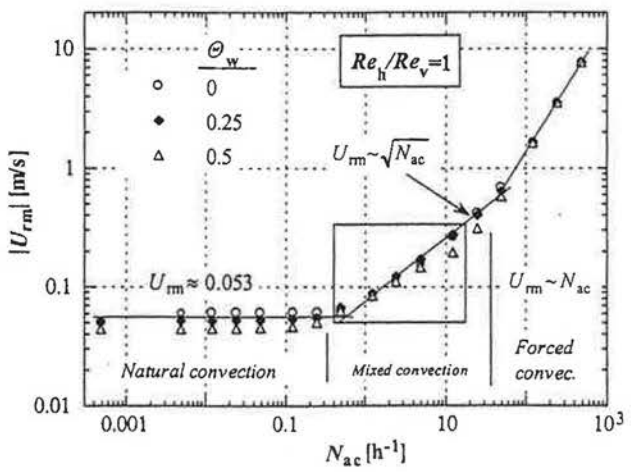

Fig. 14. Influence of the temperature of the walls Θ_w on the maximum velocity in the return flow U_{rm}, as a function of the air exchange rate N_{ac}, for equal jet flow rates (i.e., $Re_h/Re_v = 1$). ($L/H = 3$, $d/H = 0.02$; $H = 3$ m.).

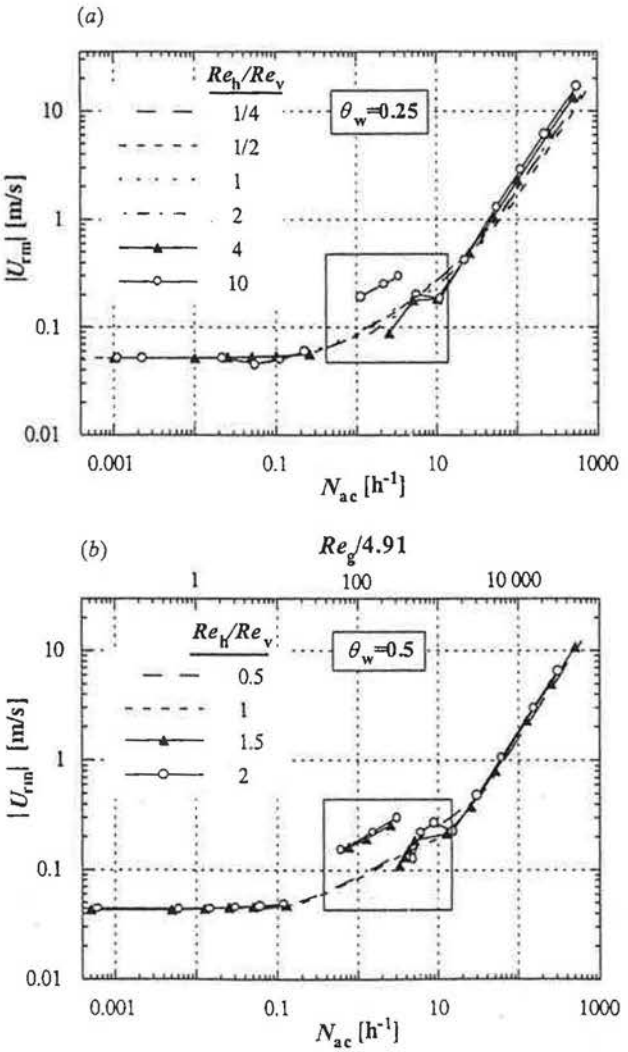

Fig. 15. Influence on U_{rm} of varying the ratio of the horizontal to the vertical jet Reynolds numbers Re_h/Re_v: (a) $\Theta_w = 0.25$ and (b) $\Theta_w = 0.5$. Symbols ▲ and ○ represent the values of Re_h/Re_v for which flow reversal occurs. In (a), no data were plotted for $Re_h/Re_v = 4$, in the range $N_{ac} = 0.25$–2.5 h^{-1}, because no satisfactorily converged solutions were obtained. ($L/H = 3$, $d/H = 0.02$; $H = 3$ m.).

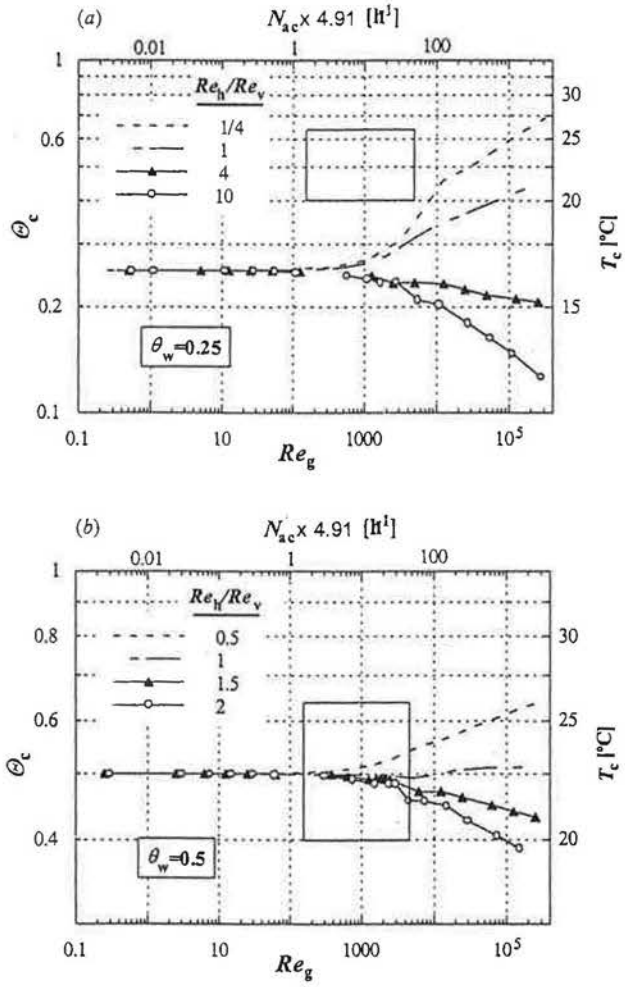

Fig. 16. Variation with the flow regime of the temperature at the centre of the room, for different Re_h/Re_v, and (a) $\Theta_w = 0.25$, (b) $\Theta_w = 0.5$. The inner frames represent the normally recommended limits for N_{ac} and for the indoor ambient temperature. ($L/H = 3$, $d/H = 0.02$; $H = 3$ m.).

sal in the mixed convection flow regime. In such cases, the "reversed" flow pattern was very similar to the one represented in Fig. 2 ($Re_h/Re_v = 1.8$, $\Theta_w = 0.53$). Besides allowing to conclude that the value of U_{rm} almost doubles relatively to a clockwise circulation flow pattern at a similar ventilation rate, Fig. 2(a)–(d) suggested the set of conditions that support the definitive "downfall" of the horizontal jet (and, therefore, the flow reversal), namely: (i) a relatively warm indoor ambient — thus reinforcing the adverse buoyancy forces acting on it —, which is promoted by a higher Θ_w; (ii) higher cold (horizontal) jet than warm (vertical) jet airflow rate, i.e., $Re_h/Re_v > 1$.

In fact, these assertions can be more precisely inferred from Fig. 15(a) and (b). It is seen here that, for a certain ventilation rate N_{ac}, the maximum velocity in the return flow is not significantly affected by changing Θ_w or Re_h/Re_v, except when the *flow reversal* occurs (in the box-limited zone), i.e.: for $Re_h/Re_v \geq 4$, if $\Theta_w = 0.25$, and for $Re_h/Re_v \geq 1.5$, if $\Theta_w = 0.5$. In such cases, the value of U_{rm} practically doubles, with the potential risk of thermal discomfort. However, considering simultaneously the recommended intervals for the room air temperature (generally, between 20 and 26°C [27]) and for the air exchange rate, N_{ac} (cf. the box-limited zones in Fig. 16(a) and (b)), it may be concluded that such risks of discomfort by flow reversal should typically be expected in Summer situations, i.e., when the temperature of the walls is relatively high and heating (vertical jet) is dispensable ($Re_h/Re_v \to \infty$).

Finally, in Fig. 17(a)–(e), a sequence of streamline patterns is presented, as obtained for $\Theta_w = 0.5$, $Re_h/Re_v = 2$ and increasing airflow rates that ranged from the natural (a) to the forced convection (e) flow regimes, passing through a complete flow reversal (c) in the mixed convection regime. It is interesting to note that, in the transitions between direct–reversed–direct rotations of the main recirculation (corresponding, approximately to the transitions between flow regimes), flow patterns appear that are qualitatively similar in the sense that they are divided into two main recirculating cells rotating oppositely (cf. Fig. 17(b) and (d)).

4. Conclusions

Using a previously validated 2-D calculation code, an extensive parametric study was conducted to determine the influence of the most relevant geometrical, dynamic and thermal parameters on the structure of the turbulent airflow inside a compartment that is typically equipped with a two-jet heating–ventilation system. A wide range of velocities was covered. The dimensional plots of the variations of U_{rm}, the maximum velocity in the return flow, as a function of the air exchange rate, N_{ac}, allowed a clear identification of the different flow regimes, ranging from natural to forced convection. Evidence was shown that the range of ventilation rates that are commonly required for acceptable thermal comfort and indoor air quality in residential buildings lies in the mixed convection flow regime, where U_{rm} varies approximately with $N_{ac}^{0.5}$. The effects of varying the room geometry, the jet inlet sections, the temperature of the walls and the ratio between ventilation and heating airflow rates were quantified and discussed in detail. The results showed that, for a given room geometry and a fixed airflow rate (low to moderate, i.e., $Re_g <$ 3000–4000), it is possible to find an optimum width of the jet inlet sections, d_{opt}, which allows a minimum U_{rm}. In the mixed-convection regime (thus, with relevance for room ventilation), the airflow structure can be strongly modified by the effect of adverse buoyancy forces. A complete flow reversal can then occur if particular conditions are associated, namely: (i) inherently low-to-moderate momentum of the jets, (ii) significant temperature difference between the walls and the incoming cold air,

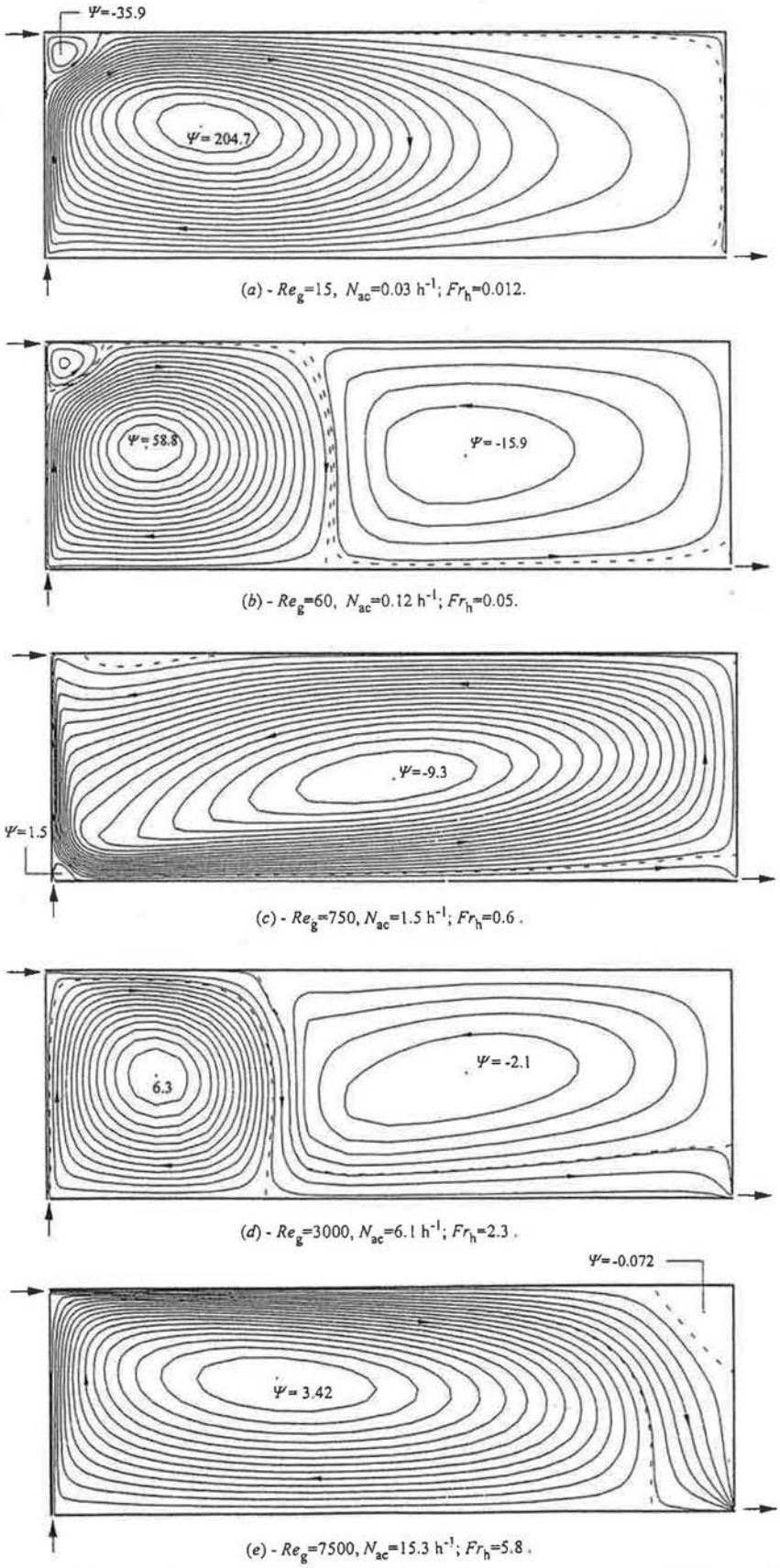

(a) - Re_g=15, N_{ac}=0.03 h^{-1}; Fr_h=0.012.

(b) - Re_g=60, N_{ac}=0.12 h^{-1}; Fr_h=0.05.

(c) - Re_g=750, N_{ac}=1.5 h^{-1}; Fr_h=0.6 .

(d) - Re_g=3000, N_{ac}=6.1 h^{-1}; Fr_h=2.3 .

(e) - Re_g=7500, N_{ac}=15.3 h^{-1}; Fr_h=5.8 .

Fig. 17. Streamline patterns obtained for $\Theta_w = 0.5$ and $Re_h/Re_v = 2$, as Re_g is successively increased. ($L/H = 3$, $d/H = 0.02$; $H = 3$ m.).

and (iii) ratio of the horizontal (cold) to the vertical (warm) jet flow rates greater than unity. In a practical situation, the flow reversal may present a risk of thermal discomfort, since the level of the maximum velocity in the occupied zone is doubled relatively to a clockwise circulating flow pattern at a similar ventilation rate. Such risk should be considered mainly for typical Summer conditions, i.e., when the temperature of the walls is relatively high and the heating (vertical jet) is unnecessary ($Re_h/Re_v \rightarrow \infty$).

5. Nomenclature

a_0	area of the jet inlet section [m^2]
Ar_g	global Archimedes number [$= g\beta(T_o - T_h)H/U_c^2$]
$C_{\varepsilon 1}$, $C_{\varepsilon 2}$, $C_{\varepsilon 3}$	constants of turbulence model
C_μ	constant of turbulence model
d, d_j	jet slot width [m]
D_k, E_ε	extra-terms in the k and ε equations
f_μ, f_1, f_2	functions of low-Re k–ε models
Fr_j	jet Froude number {$= U_j/[g\beta d_j(T_v - T_h)]^{1/2}$}
g_i	gravitational acceleration in the i-direction [$m \cdot s^{-2}$]
G_k	rate of buoyancy production/destruction of turbulence kinetic energy [$m^2 \cdot s^{-3}$]
Gr_H	Grashof number [$= g\beta(T_o - T_h)H^3/\nu^2$]
H	room height [m]
I_t	turbulence intensity {$= [(\overline{u'^2} + \overline{v'^2})/2]^{1/2}/U_c$, from measurements; or $= (2k/3)^{1/2}/U_c$, from calculations}
k	turbulence kinetic energy ($= \overline{u_i' u_i'}/2$) [$m^2 \cdot s^{-2}$]
L	room length [m]
L_c	characteristic length ($= d_h + d_v$) [m]
p	pressure [$N \cdot m^{-2}$]
p_{ef}	$= p + 2/3\rho k$, for numerical convenience [$N \cdot m^{-2}$]
P_k	rate of shear production of k [$m^2 \cdot s^{-3}$]
Pr/Pr_t	molecular/turbulent Prandtl number
Re_g	global Reynolds number ($= U_c L_c/\nu$)
Re_j	jet Reynolds number ($= U_j d_j/\nu$)
Re_t	local-turbulence Reynolds number ($= k^2/\nu\tilde{\varepsilon}$)
S_ϕ	source-term in Eq. (3)
T	temperature [°C]
T_{ref}	reference temperature [$= (T_h + T_v)/2$] [°C]
u, v	mean velocity components [$m \cdot s^{-1}$]
u_i	mean velocity in the i-direction [$m \cdot s^{-1}$]
u_τ	friction velocity [$= (\tau_w/\rho)^{1/2}$] [$m \cdot s^{-1}$]
U_c	characteristic velocity scale {$= (U_h d_h + U_v d_v)/(d_h + d_v)$} [$m \cdot s^{-1}$]
U_h (U_v)	horizontal (vertical) jet velocity [$m \cdot s^{-1}$]
U_{rm}	maximum velocity in the return flow [$m \cdot s^{-1}$]
x, y	spatial coordinates (cf. Fig. 1) [m]
x_n	normal distance to the nearest wall [m]
x_n^+	dimensionless wall-distance ($= u_\tau x_n/\nu$)

Greek symbols

α	molecular thermal diffusibility [$m^2 \cdot s^{-1}$]
α_t	turbulent thermal diffusibility [$m^2 \cdot s^{-1}$]
β	thermal expansion coefficient [K^{-1}]
ε, $\tilde{\varepsilon}$	dissipation rate of k ($\tilde{\varepsilon} = \varepsilon + D_k$) [$m^2 \cdot s^{-3}$]
ϕ	generic variable
Γ_ϕ	diffusibility in mean-flow equations
κ	von Karman constant ($= 0.4187$)
ν	molecular kinematic viscosity [$m^2 \cdot s^{-1}$]
ν_t	turbulent kinematic viscosity [$m^2 \cdot s^{-1}$]
μ	fluid dynamic viscosity ($= \rho\nu$) [$N \cdot s \cdot m^{-2}$]
Θ	dimensionless temperature [$= (T - T_h)/(T_v - T_h)$]
ρ	fluid density [$kg \cdot m^{-3}$]
σ_k, σ_ε	constants of turbulence model
τ_t	turbulent shear stress, ($= -\rho\overline{u'v'}$) [$N \cdot m^{-2}$]
τ_w	wall shear stress {$= \mu(du/dx_n)_w$} [$N \cdot m^{-2}$]
ψ	stream function [$m^2 \cdot s^{-1}$] (dimensionless: $\Psi = \psi/(U_c L_c)$)

Superscripts

′	fluctuating quantity
+	dimensionless wall variables

Subscripts

c	centre of the room
h	horizontal jet
in	inlet condition
i, j	spatial indices
j	generic jet
n	direction normal to a surface
o	outlet condition
t	turbulent
v	vertical jet
w	wall condition
0	jet inlet section

References

[1] Q. Chen, Q.Z. Jiang, Significant questions in predicting room air motion, ASHRAE Trans. 98 (1) (1992) 929–939.
[2] B.E. Launder, D.B. Spalding, The numerical computation of turbulent flows, Comp. Methods Appl. Mech. Eng. 3 (1974) 269–289.
[3] P.V. Nielsen, Flow in air conditioned rooms, Danfoss, Denmark, English Translation of PhD Thesis, Technical University of Denmark, 1974.

[4] A. Restivo, Turbulent Flow in Ventilated Rooms, PhD Thesis, Dept. Mech. Eng., Imperial College of Science and Technology, London, 1979.
[5] P.V. Nielsen, A. Restivo, J.H. Whitelaw, The velocity characteristics of ventilated rooms, J. Fluids Eng. 100 (1978) 291–298.
[6] P.V. Nielsen, A. Restivo, J.H. Whitelaw, Buoyancy-affected flows in ventilated rooms, Numer. Heat Transfer 2 (1979) 115–127.
[7] A.D. Gosman, P.V. Nielsen, A. Restivo, J.H. Whitelaw, The flow properties of rooms with small ventilation openings, J. Fluids Eng. 102 (1980) 316–323.
[8] G.E. Whittle, Computation of air movement and convective heat transfer within buildings, Int. J. Ambient Energy 7 (3) (1986) 151–164.
[9] S.V. Patankar, Numerical Heat Transfer and Fluid Flow, Hemisphere Publishing, Washington, DC, 1980.
[10] M. Skovgaard, P.V. Nielsen, Numerical prediction of air distribution in rooms with ventilation of the mixing type using the standard $k-\varepsilon$ model, Paper no. 13 — Indoor Environmental Technology, Institute of Building Technology and Structural Engineering, Aalborg University, Denmark, 1990.
[11] P.V. Nielsen, Models for the prediction of room air distribution, Paper no. 20 — Indoor Environmental Technology, Institute of Building Technology and Structural Engineering, Aalborg University, Denmark, 1991 (Presented in the 12th AIVC Conference on Air Movement and Ventilation Control within Buildings, Ottawa, Canada, 1991).
[12] V.C. Patel, W. Rodi, G. Scheuerer, Turbulence models for near-wall and low-Reynolds number flows: a review, AIAA J. 23 (9) (1985) 1308–1318.
[13] Q. Liu, S.J. Hoff, G.M. Maxwell, D.S. Bundy, Comparison of three $k-\varepsilon$ turbulence models for predicting ventilation air jets, Trans. ASAE 39 (2) (1996) 689–698.
[14] L. Davidson, Calculation of the turbulent buoyancy-driven flow in a rectangular cavity using an efficient solver and two different low Reynolds number $k-\varepsilon$ turbulence models, Numer. Heat Transfer, Part A 18 (1990) 129–147.
[15] H.B. Awbi, Calculation of convective heat transfer coefficients of room surfaces for natural convection, Energy and Buildings 28 (1998) 219–227.
[16] D. Blay, S. Mergui, C. Niculae, Confined turbulent mixed convection in the presence of a horizontal buoyant wall jet, in: Fundamentals of Mixed Convection, Trans. ASME HTD vol. 213 1992, pp. 65–72.
[17] J.J. Costa, S. Mergui, J.L. Tuhault, F. Penot, D. Blay, L. Oliveira, Test of turbulence models for the numerical simulation of internal mixed convection flows, in: ROOMVENT'92 — 3rd International Conference on Air Distribution in Rooms, Aalborg, Denmark 11992, pp. 159–175.
[18] Q. Chen, Comparison of different $k-\varepsilon$ models for indoor air flow computations, Numer. Heat Transfer, Part B 28 (1995) 353–369.
[19] J.J. Costa, L.A. Oliveira, D. Blay, Test of several versions for the $k-\varepsilon$ type turbulence modelling of internal mixed convection flows, Int. J. Heat Mass Transfer 42 (1999) 4391–4409.
[20] C.C. Chieng, B.E. Launder, On the calculation of turbulent heat transport downstream from an abrupt pipe expansion, Numer. Heat Transfer 3 (1980) 189–207.
[21] Y. Nagano, M. Hishida, Improved form of the $k-\varepsilon$ model for wall turbulent shear flows, J. Fluids Eng. 109 (1987) 156–160.
[22] D.D. Gray, A. Giorgini, The validity of the Boussinesq approximation for liquids and gases, Int. J. Heat Mass Transfer 19 (1976) 545–551.
[23] T. Cebeci, A. Khattab, Prediction of turbulent-free-convective-heat transfer from a vertical flat plate, J. Heat Transfer (1975) 469–471.
[24] R.A. Henkes, Natural-convection boundary layers, PhD Thesis, Faculty of Applied Physics, Delft University of Technology, The Netherlands, 1990.
[25] J.P. Van Doormaal, G.D. Raithby, Enhancements of the SIMPLE method for predicting incompressible fluid flows, Numer. Heat Transfer 7 (1984) 147–163.
[26] B. Delenne, G. Pot, Modelling of the turbulent boundary layer implemented in CFD code N3S and application to flows in heated rooms, in: 8th International Conference on Numerical Methods in Thermal Problems, Swansea, UK vol. VIII 1993, pp. 670–681, 1.
[27] S. Mergui, Experimental characterisation of natural and mixed convection airflows within a closed cavity, PhD Thesis, University of Poitiers, France, 1993 (in French).
[28] H.B. Awbi, Scale effect in room airflow study, Energy and Buildings 14 (1990) 207–210.
[29] P.V. Nielsen, Numerical prediction of air distribution in rooms — status and potentials, in: L. Christianson (Ed.), Building Systems: Room Air and Air Contaminant Distribution, American Society of Heating, Refrigerating and Air-Conditioning Engineers (ASHRAE), Atlanta, GA, USA, 1989, pp. 31–38.
[30] Guidelines for Ventilation Requirements in Buildings, Report no. 11, European Concerted Action — Indoor Air Quality and its Impact on Man, Commission of the European Communities, 1992.
[31] ASHRAE Standard 55, Thermal environmental conditions for human occupancy, Atlanta, GA, USA, 1992.
[32] ISO Standard 7730, Moderate thermal environments — Determination of the PMV and PPD indices and specification of the conditions for thermal comfort, International Standards Organisation, Geneve, Switzerland, 1994.